Normal modes of a small bilayer system of binary classical charged particles trapped in a parabolic confinement potential

Xin Lu,[1,*] Baowen Li,[2,3] and Chang-Qin Wu[1]

[1]*Surface Physics Laboratory (National Key Laboratory) and Department of Physics, Fudan University, Shanghai 200433, People's Republic of China*

[2]*NUS Graduate School for Integrative Sciences and Engineering, Singapore 117597, Republic of Singapore*

[3]*Department of Physics and Centre for Computational Science and Engineering, National University of Singapore, Singapore 117542, Republic of Singapore*

(Received 11 June 2008; published 2 October 2008)

The normal modes and the melting character of a bilayer system consisting of binary charged particles with different charge and/or different mass, interacting through a Coulomb potential and confined in a parabolic trap are investigated. The normal mode spectrum is discussed as a function of the charge ratio (CR) and mass ratio (MR) of the two kinds of charged particles as well as the interlayer separation. We show that the dependence of the normal modes on the excited states can be tuned by varying the CR, the MR, and the interlayer distance. Once the interlayer distance is larger than a critical value, the first excited state corresponds only to the intershell rotation mode. In addition, the intershell rotation melting temperature is discussed as a function of the CR and MR as well as the interlayer separation.

DOI: 10.1103/PhysRevE.78.041401 PACS number(s): 82.70.Dd, 68.65.Ac, 61.50.−f, 52.27.Lw

I. INTRODUCTION

There has been considerable progress in theoretical and experimental studies of the properties of a cluster containing classical particles trapped in a two-dimensional artificial external potential during recent decades [1–8]. The theoretical models are applicable to many real systems such as dusty plasmas [1,2], electrons in the top surface of liquid helium [3–6], colloidal suspensions [7], electrons in quantum dot structures [8], etc. The characteristics of systems consisting of one-component particles has been investigated both theoretically and experimentally in many previous studies [9–26]. A remarkable diversity of new binary structures has been obtained in a recent experiment studying confined oppositely charged particles [27]. For binary single-layer systems, the possibility of predicting the appearance of intershell rotation based on the configuration and the number ratio of two types of particle has been discussed theoretically [28,29]. Furthermore, the important parameters [e.g., the charge ratio (CR) and mass ratio (MR) of the two kinds of particles] determining the occurrence of a structural phase transition [30] and the melting behavior of a two-dimensional (2D) binary cluster confined in hard-wall traps [31] have been studied in detail. For one-component bilayer systems, the structure and dynamical properties as well as the melting characteristics of both the classical bilayer Coulomb cluster [32] and the classical bilayer crystal of dipoles [33] have been adequately studied. This work indicates that the dynamical properties of bilayer systems are strongly independent of the interlayer distance and the density of particles in each layer.

The main purpose of this work is to investigate the normal modes of an artificial bilayer system with the same number of particles in each layer trapped by a parabolic confinement potential. The particles in each layer form a configuration with a clear single shell. We want to find the relations between the normal modes, melting properties, and dominant parameters of the system. One of the most important normal modes is the intershell rotation (ISR) which usually corresponds to the first excited state of a small single-layer system consisting of one-component particles confined in a parabolic trap [20]. In this work, we consider a bilayer system consisting of two types of charged particles (with different charge or mass) distributed one in each of two layers. We find that the normal modes and the rotation melting between the two shells of the system can be adjusted by changing the CR and MR of the two species of particles as well as the interlayer separation, so that the dynamical character of the particles in one layer can be determined by the properties of the particles in the other layer. It should be noticed that the structural transition behavior of binary particles in a single layer has been studied adequately in Ref. [30]. In the current work, we do not consider the structural transition occurring at small interlayer separation where the shell structure can be destroyed.

The paper is organized as follows. In Sec. II our model for a bilayer system consisting of binary charged particles is introduced and the numerical process for finding the energy and normal spectral of the ground state configurations is described. In Sec. III the results for the normal modes and melting temperature of the bilayer system with different CR and MR of the two types of particles are shown. In Sec. IV the conclusion is given.

II. MODEL

We consider an ideal model of a bilayer system which consists of $N=N_A+N_B$ charged particles. There are N_A (N_B) particles with charge q_A (q_B) and mass m_A (m_B) located in layer A (B). The interlayer distance is l. The interparticle

*xglu@fudan.edu.cn. Present address: Department of Physics and Centre for Computational Science and Engineering, National University of Singapore, Singapore 117542, Republic of Singapore.

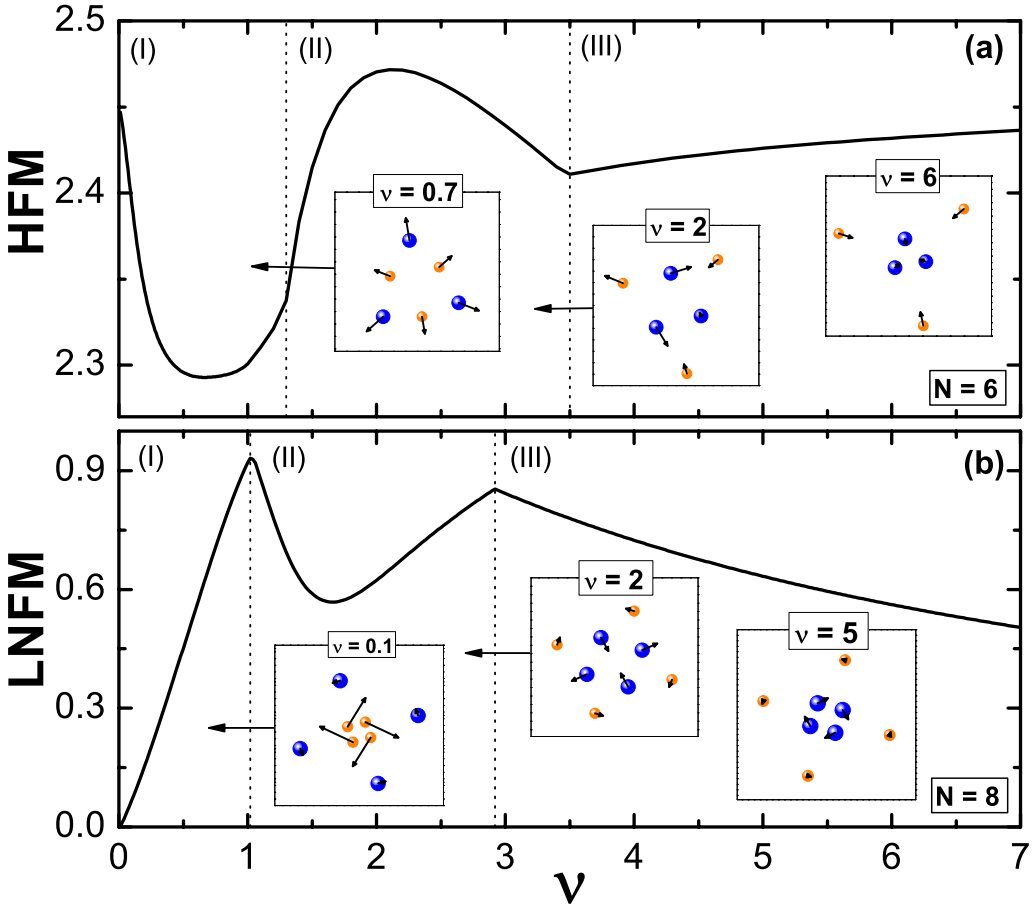

FIG. 1. (Color online) (a) HFM for the cluster of $C^{3,3}$ with $l=0.5$ and (b) LNFM for the cluster of $C^{4,4}$ with $l=1$ as functions of ν. The insets indicate the normal modes in different regions of ν. The particles in layers A and B are denoted by big blue (dark gray) and small orange (light gray) balls, respectively.

interaction is a pure Coulomb potential and all particles are trapped by a parabolic confinement potential. The Hamiltonian of the system is given by

$$\begin{aligned} H &= H_{\mathrm{tr}}^{A} + H_{\mathrm{tr}}^{B} + H_{\mathrm{cc}}^{A} + H_{\mathrm{cc}}^{B} + H_{\mathrm{cc}}^{AB} \\ &= \sum_{i=1}^{N_A} \frac{1}{2} m_A \omega_0^2 r_i^2 + \sum_{j=1}^{N_B} \frac{1}{2} m_B \omega_0^2 r_j^2 + \frac{q_A^2}{\epsilon} \sum_{i>i'=1}^{N_A} \frac{1}{|\mathbf{r}_{ii'}|} \\ &\quad + \frac{q_B^2}{\epsilon} \sum_{j>j'=1}^{N_B} \frac{1}{|\mathbf{r}_{jj'}|} + \frac{q_A q_B}{\epsilon} \sum_{i=1}^{N_A} \sum_{j=1}^{N_B} \frac{1}{|\tilde{\mathbf{r}}_{ij}|}, \end{aligned} \tag{1}$$

where $H_{\mathrm{tr}}^{A(B)}$ describes the parabolic potential confining $N_{A(B)}$ charged particles, $H_{\mathrm{cc}}^{A(B)}$ represents the interaction potential of type A (B) particles, H_{cc}^{AB} is the interaction potential between the two kinds of particles, ϵ is the dielectric constant, $r_i = |\mathbf{r}_i|$ is the distance of the ith particle from the center of the confinement potential, $|\mathbf{r}_{ii'}| = |\mathbf{r}_i - \mathbf{r}_{i'}|$ denotes the distance between the particles i and i' in the same layer, and $|\tilde{\mathbf{r}}_{ij}| = (|\mathbf{r}_i - \mathbf{r}_j|^2 + l^2)^{1/2}$ indicates the distance between the ith particle in layer A and the jth particle in layer B. We rewrite the energy and the distances in units of $E_0 = (m_A \omega_0^2 q_A^4 / 2\epsilon^2)^{1/3}$ and $r_0 = (2q_A^2 / \epsilon m_A \omega^2)^{1/3}$, respectively. Then the dimensionless Hamiltonian is

$$H = \sum_{i=1}^{N_A} r_i^2 + \mu \sum_{j=1}^{N_B} r_j^2 + \sum_{i>i'=1} \frac{1}{|\mathbf{r}_{ii'}|} + \sum_{j>j'=1}^{N_B} \frac{\nu^2}{|\mathbf{r}_{jj'}|} + \sum_{i=1}^{N_A} \sum_{j=1}^{N_B} \frac{\nu}{|\tilde{\mathbf{r}}_{ij}|}, \tag{2}$$

where $\nu = q_B / q_A$ describes the CR and $\mu = m_B / m_A$ denotes the MR. To obtain the ground state configuration of the system, we use the standard Monte Carlo simulation (with the Metropolis algorithm) [34]. The one with the lowest energy from the stable states obtained is taken as the ground state configuration. To check the stability of a configuration, we calculate the eigenvalues of the dynamical matrix defined as

$$H_{\alpha\beta,ij} = \frac{\partial^2 H}{\partial r_{\alpha,i} \partial r_{\beta,j}}, \tag{3}$$

which gives the square of the frequencies of the normal modes of the system ($\alpha, \beta = x, y$, and i, j denote the particle indices), where the Householder diagonalization technique is used [20]. When all the squared frequencies are positive, the configuration is taken as a stable state.

III. NUMERICAL RESULTS

In this section, we will present the results for the normal modes of a system with $N=4,6,8,10$ particles, where we

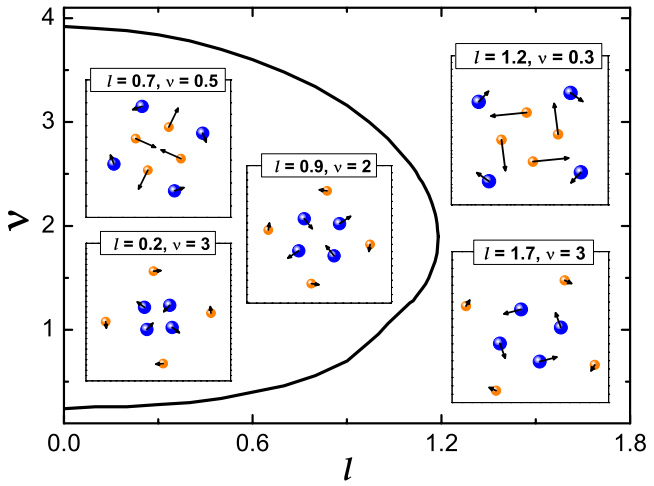

FIG. 2. (Color online) Critical values of ν distinguishing the ISR and the non-ISR of the LNFM as a function of the interlayer separation for a cluster of $N=8$ particles. The normal modes corresponding to different regions of ν at certain interlayer distances are shown in the insets. The particles in layers A and B are denoted by big blue (dark gray) and small orange (light gray) balls, respectively.

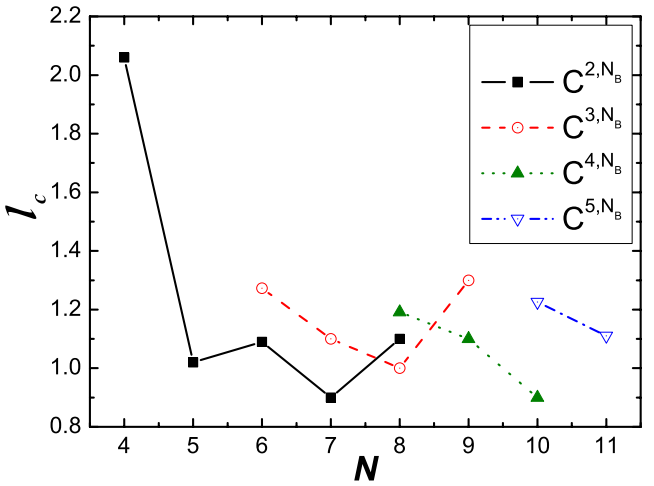

FIG. 3. (Color online) Critical value of the interlayer distance where the non-ISR disappears as a function of N for different ratios of numbers between the particles in layer A and the particles in layer B.

focus on the characteristics of the lowest nonzero frequency mode (LNFM) and the highest frequency mode (HFM). Then we will describe the shearlike and compressionlike modes of the system with $N=6$ and 8 particles. Finally, we pay attention to the intershell rotation melting of the system with $N=4,6,8,10$ particles.

A. Lowest nonzero frequency mode and highest frequency mode

For a system consisting of any number of particles trapped in a parabolic potential, the rotation of the whole system mode (RSM) corresponds to the lowest frequency $\omega=0$. Meanwhile, if all particles have identical mass, the system has the frequency $\omega=\sqrt{2}$ which corresponds to the center of mass mode (CMM). It is obvious that the RSM and CMM are independent of the CR of the two kinds of particles. Here, we concentrate on the lowest nonzero frequency mode and the highest frequency mode of the system.

From the work in Ref. [20], the ISR is found as the LNFM of the cluster containing a small number of particles. For the current bilayer system, the LNFM corresponds not only to the ISR but also to the formation of a vortex-antivortex pair (VAP). Figure 1(b) shows the LNFM for the system $C^{4,4}$ (in the form C^{N_A,N_B}) at the interlayer distance $l=1$ as a function of the CR of the two kinds of particles. The normal modes in each region of ν are shown in the insets. We find that the LNFM corresponds to ISR in region I and III, and to a VAP in region II with distinct shell configurations. In region I, the LNF increases with ν, due to the effect of the interlayer repulsive interaction, i.e., the difference of the radius of the two shells decreases with increasing ν, and consequently the coupling between the two layers becomes stronger and the energy needed to excite the intershell rotation mode becomes larger. The opposite feature is shown in region III, where the LNF decreases with increasing ν. This behavior can be understood through the fact that, as the separation of the two shells increases with the value of ν, the coupling between the layers becomes weaker, which leads to decreasing energy exciting the ISR. This feature is also observed for other systems of $N=4,6,10$ particles.

Similarly, in Fig. 1(a) we show the HFM as a function of ν for the system $C^{3,3}$ at $l=0.5$. Usually, the HFM is the breathing mode for very small single-layer systems [23]. In our system, as shown in the insets of Fig. 1(a), only regions I and III correspond to the breathing mode, while region II corresponds to a localized relative motion of two pairs of particles due to the strong restoring force coming from the change of the interparticle distance.

To analyze the effect of the interlayer distance on the first excited state, we plot the boundary values of ν distinguishing ISR and non-ISR of the LNFM for the system $C^{4,4}$ as a function of l in Fig. 2. We can see that, when the interlayer separation is small, only very small and very large values of ν correspond to ISR, while the middle range of ν corresponds to other formations (e.g., the VAP shown in the insets). With the increase of l, the range of ν corresponding to ISR becomes wider. Once the interlayer separation is above a critical value, the mode of non-ISR disappears, and the LNFM corresponds only to ISR, no matter the value of ν. That feature results from weak coupling between the two layers at large l. Similarly, we can expect that, once the interlayer distance is large enough, the HFM only corresponds to the breathing mode. Because to the LNF is closely linked to the stability of the ground state configuration and the melting properties of the system [20,30], we can say that the stability of the bilayer system depends not only on the CR of the two kinds of particles, but also on the interlayer separation.

For the system $C^{4,4}$, the critical value of the interlayer distance l_c where the non-ISR begins to disappear is 1.191. The relation between the critical value and the size of the system is shown in Fig. 3. In the plot, the curves with dif-

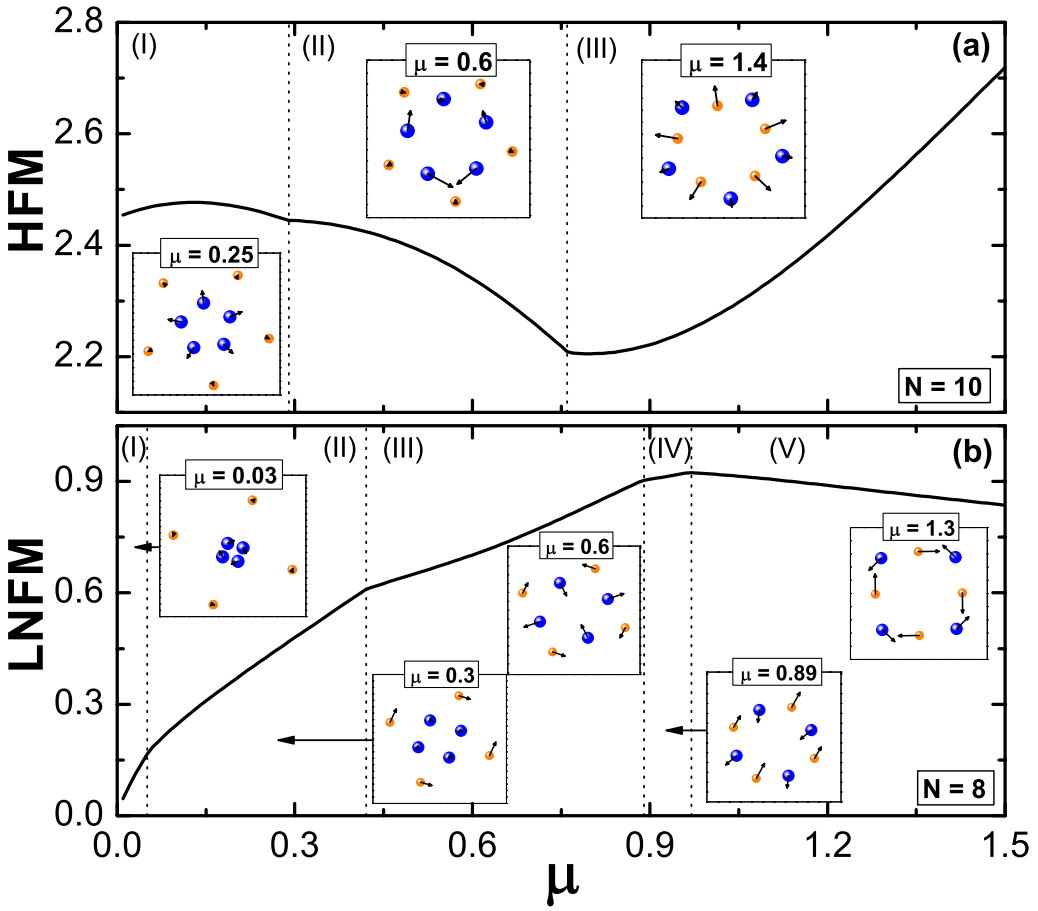

FIG. 4. (Color online) (a) HFM for a system of $N=10$ particles and (b) LNFM for a system of $N=8$ particles as functions of μ. The insets indicate the normal modes in different regions of μ. The particles in layers A and B are denoted by big blue (dark gray) and small orange (light gray) balls, respectively.

ferent styles indicate the systems C^{2,N_b}, C^{3,N_B}, C^{4,N_B}, and C^{5,N_B}, respectively. For the system C^{2,N_B}, as an example, l_c decreases with increasing size of the system (i.e., increase of the number N_B) except for the systems $C^{2,4}$ and $C^{2,6}$. Similar characteristics can be found in the systems C^{3,N_B}, C^{4,N_B}, and C^{5,N_B}. We find that $l_c^{2,4}$ (in the form of $l_c^{N_A,N_B}$) and $l_c^{2,6}$ are larger than $l_c^{2,3}$ and $l_c^{2,5}$, in the respect that, at a certain interlayer distance, a ringlike bilayer structure with compatible numbers of particles located in different shells is more stable against ISR motion (i.e., the ratio of N_B to N_A is integer). A similar feature is also presented as $l_c^{3,6} > l_c^{3,5}$. Furthermore, we find that the behaviors of l_c still keep to the above rule even for systems with the same number of total particles, such as $l_c^{3,6} > l_c^{4,5}$, $l_c^{4,4} > l_c^{3,5}$, $l_c^{2,6} > l_c^{3,5}$, and $l_c^{5,5} > l_c^{4,6}$. In addition, although both systems $C^{2,4}$ and $C^{3,3}$ have compatible numbers of particles, but we find that $l_c^{3,3} > l_c^{2,4}$, and a similar behavior is also represented as $l_c^{4,4} > l_c^{2,6}$. That feature tells us that a system with the same number of particles in each shell is more stable against ISR motion than other bilayer systems in ringlike configurations with the same N at a certain interlayer separation.

Then we will discuss the behaviors of the HFM and LNFM for systems consisting of particles with different masses. As an example, Fig. 4(a) shows the HFM as a function of μ for the system $C^{5,5}$ at the interlayer distance $l=1$. According to the different modes, the interval of μ is divided into three regions. The regions I and III correspond to the breathing mode, while region II corresponds to the localized relative motion. When l is large enough, the HFM should only correspond to the breathing mode, which is similar to the relation between HFM and ν. The LNFM as a function of μ for the system $C^{4,4}$ at the interlayer separation $l=1$ is shown in Fig. 4(b). The interval of μ is divided into five regions according to the normal modes in each region. Regions I and V correspond to the ISR, while regions II, III, and IV correspond to different types of the formation of VAP as shown in the insets. Be analogous to the case of different CR, a similar behavior can be also found in the relation between the interlayer distance and the critical values of μ distinguishing the ISR mode of LNFM or the breathing mode of HFM. Furthermore, the feature of the stability against the ISR motion for varying MR is also similar to the condition of variable CR as shown in Fig. 3.

B. Shearlike and compressionlike modes

For separating the compressional and shear contributions of the LNFM and HFM, we consider the z component of the rotor $\Psi_r(k)=\mathbf{e}_z\cdot\mathrm{rot}\,\Psi(k)$ and the divergence $\Psi_d(k)=\mathrm{div}\,\Psi(k)$ of the field of eigenvectors for different modes k [21],

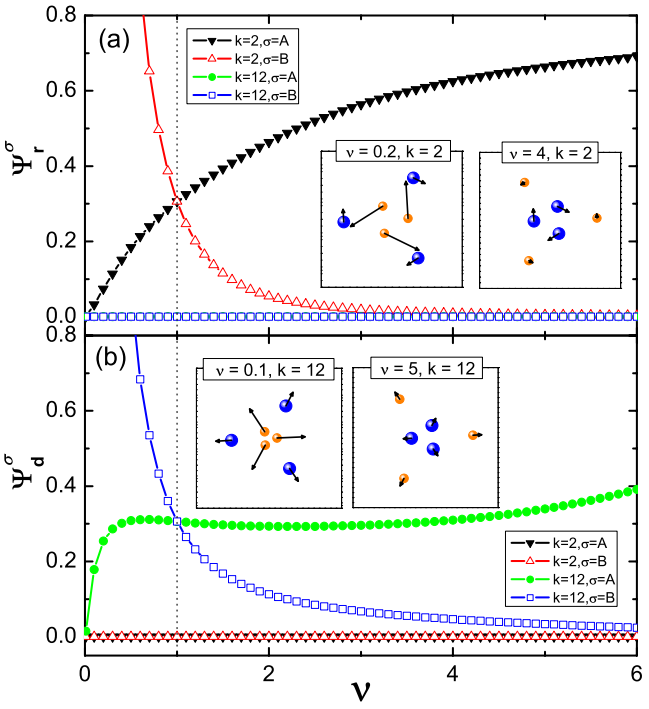

FIG. 5. (Color online) Distribution of (a) the rotor Ψ_r^σ and (b) the divergence Ψ_d^σ as functions of ν for the first excited state ($k=2$) and the highest excited ($k=12$) state of the system $C^{3,3}$ at $l=1.3$. The normal modes for $k=2,12$ with $\sigma=A,B$ for different values of ν are shown in the insets.

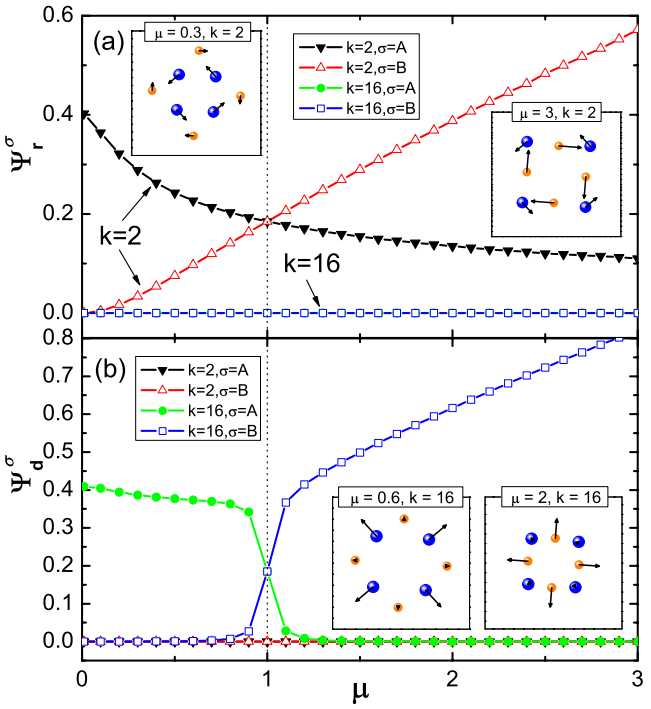

FIG. 6. (Color online) The distribution of (a) the rotor Ψ_r^σ and (b) the divergence Ψ_d^σ as a function of μ for the first excited state ($k=2$) and the highest excited ($k=16$) states of the system $C^{4,4}$ at $l=2$. The normal modes for $k=2,16$ with $\sigma=A,B$ for different values of μ are shown in the insets.

$$\Psi_r^\sigma(k) = \frac{1}{N_\sigma}\sum_{i=1}^{N_\sigma}[\psi_{r,i}^\sigma(k)]^2, \tag{4a}$$

$$\Psi_d^\sigma(k) = \frac{1}{N_\sigma}\sum_{i=1}^{N_\sigma}[\psi_{d,i}^\sigma(k)]^2, \tag{4b}$$

where $\psi_{r,i}^\sigma(k)$ and $\psi_{d,i}^\sigma(k)$ are calculated from

$$\psi_{r,i}^\sigma(k) = \frac{1}{S}\sum_{s=1}^{S}\frac{(\mathbf{r}_i^\sigma - \mathbf{r}_s^\sigma)[\rho_i^\sigma(k) - \rho_s^\sigma(k)]}{|\mathbf{r}_i^\sigma - \mathbf{r}_s^\sigma|^2}, \tag{5a}$$

$$\psi_{d,i}^\sigma(k) = \frac{1}{S}\sum_{s=1}^{S}\frac{(\mathbf{r}_i^\sigma - \mathbf{r}_s^\sigma)[\rho_i^\sigma(k) - \rho_s^\sigma(k)]}{|\mathbf{r}_i^\sigma - \mathbf{r}_s^\sigma|^2}, \tag{5b}$$

where $\mathbf{r}_s^\sigma$ is the coordinate of the sth neighboring particle to the ith particle in layer σ ($\sigma=A,B$). S is the number of the neighbors. $\rho_i^\sigma(k)$ is the eigenvector of the ith particle in layer σ for mode k.

As an example, Fig. 5 shows the rotor and divergence as functions of ν for the two representative modes: the first excited state and the highest excited state, of the system $C^{3,3}$ at the interlayer separation $l=1.3$. Here each normal mode corresponds to the same mode of motion for different values of ν by using particular interlayer distance. It is obvious that $\Psi_r^\sigma(k=12)\approx 0$ and $\Psi_d^\sigma(k=2)\approx 0$ ($\sigma=A,B$), and both of them are almost independent on the CR (also independent on the MR, as shown in Fig. 6). This feature indicates that the shearlike modes are mainly activated with lower frequency and the compressionlike modes are mostly excited with higher frequency, which also occurs in single layer cluster of charged particles [23,24]. We know from Fig. 5(a) that, with the increasing value of ν, the rotor $\Psi_r^B(k=2)$ decreases exponentially, which is similar to the behavior of the divergence $\Psi_d^B(k=12)$, due to the increasing interparticle interaction, while the value of $\Psi_r^A(k=2)$ increases since the decreasing ratio of the radius of shell A to shell B. Figure 5(b) represents an unexpectable nonmonotone changing of $\Psi_d^d(k=12)$. The divergence for the highest excited state changes sharply when ν begins to increase from zero, and then tardily decreases a little until it continues to increase again along with ν. That nonmonotonic feature comes from the strong restoring forces between the particles in layers A and B, and it can be enhanced by reducing the interlayer separation and lowered by increasing the interlayer distance until the interlayer coupling is weak enough that the divergence can become monotonic. We also find that, at $\nu=1$, $\Psi_r^A(k=2)=\Psi_r^B(k=2)\approx\Psi_d^A(k=12)=\Psi_d^B(k=12)$, since the intralayer interactions of particle A and particle B are identical. Similar characteristics can also be found in the systems $C^{2,2}$, $C^{4,4}$, and $C^{5,5}$.

Similarly, we give the rotor and the divergence as functions of μ for the two modes ($k=2,16$) of the system $C^{4,4}$ at the interlayer separation $l=2$ in Fig. 6. The method of choosing the interlayer distance is the same as for different ν mentioned above. From the figure we also find that $\Psi_r^\sigma(k=16)\approx 0$ and $\Psi_d^\sigma(k=2)\approx 0$, which are independent of μ. We find

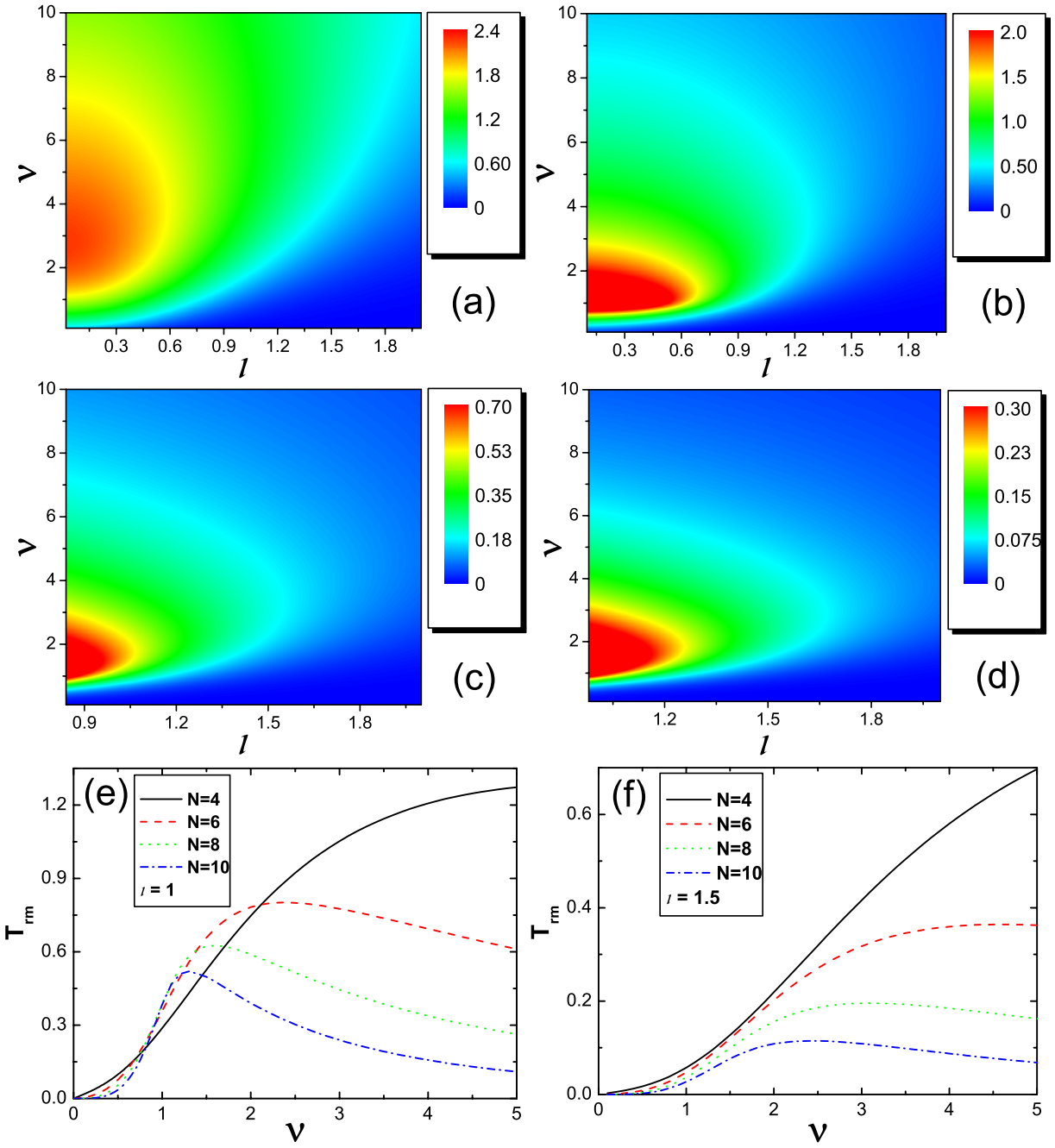

FIG. 7. (Color online) (a)–(d) Intershell rotation melting temperature for varying interlayer distance l and CR for the systems $C^{2,2}$, $C^{3,3}$, $C^{4,4}$, and $C^{5,5}$. (e), (f) Intershell rotation melting temperature as a function of ν for different systems at certain interlayer separations ($l=1,1.5$).

from Fig. 6(a) that the value of $\Psi_r^B(k=2)$ increases with μ (almost linearly in some regions of μ) due to the increasing confinement potential. Although the mass of particle A is invariable, the rotor decreases with increase of μ, owing to the increasing ratio of the radius of shell A to that of shell B. Figure 6(b) tells us that the value of $\Psi_d^B(k=16)$ increases along with μ and the value of $\Psi_d^A(k=16)$ decreases accordingly. There is an interesting behavior of the divergence: $\Psi_d^B(k=16)\approx 0$ in the region of $\mu \leqslant 0.8$ and jumps near $\mu=1$. In contrast, the value of $\Psi_d^A(k=16)$ decreases slowly when $\mu \leqslant 0.8$ and jumps down to zero near $\mu=1$. Similar behavior can also be found in the systems $C^{2,2}$, $C^{3,3}$, and $C^{5,5}$. By making use of this feature, the divergence of a shell in a layer for a high excited state can be adjusted between the two steps by changing the mass of the particles in the other layer.

The characteristics of the rotor and the divergence of the field of eigenvectors for the bilayer system mentioned above indicate that, at a certain interlayer distance, the shearlike mode and the compressionlike mode of the particles in one layer can be adjusted by changing the charge or the mass of another kind of particle in the other layer.

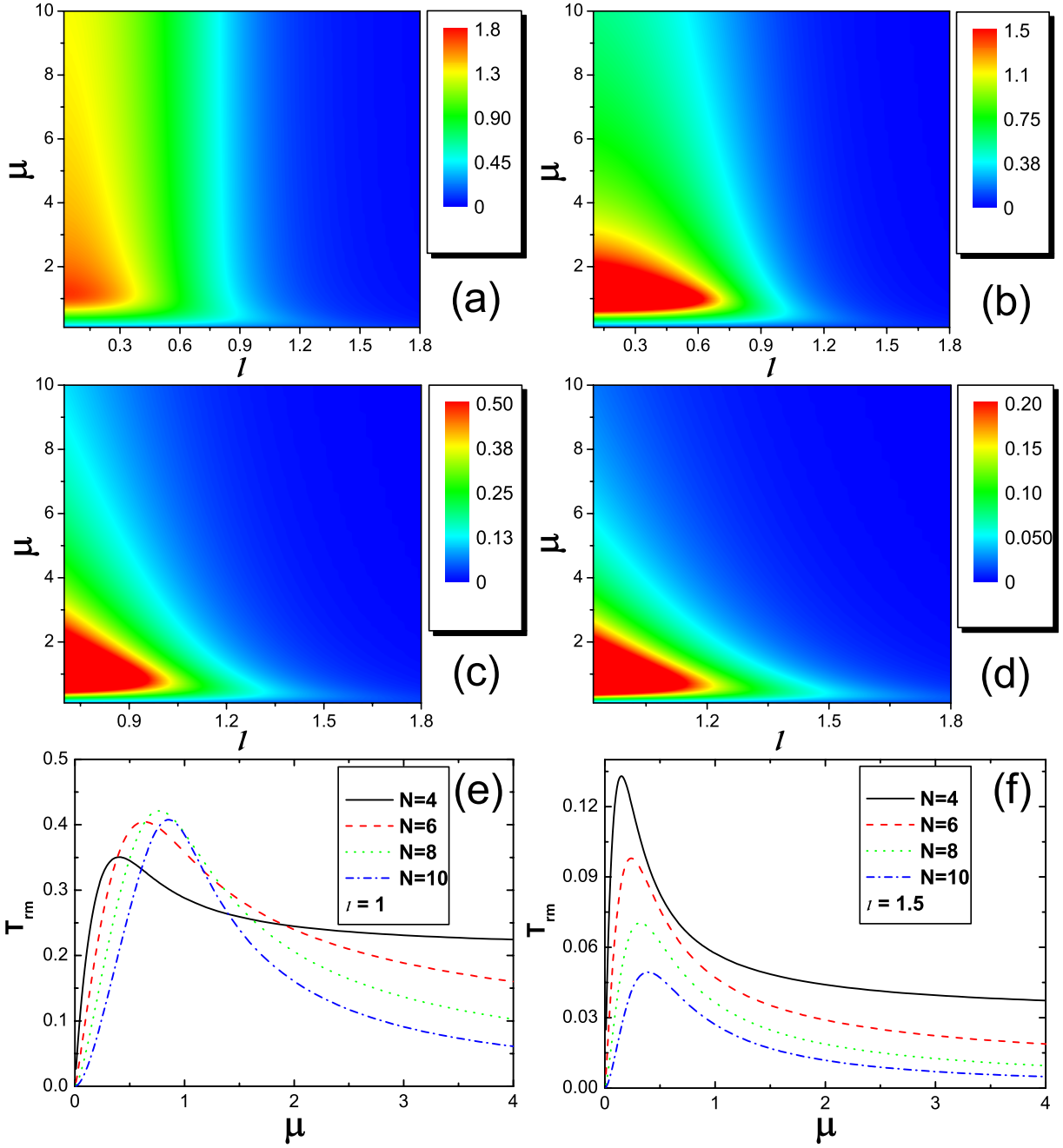

FIG. 8. (Color online) (a)–(d) Intershell rotation melting temperature for varying interlayer distance l and MR for the systems $C^{2,2}$, $C^{3,3}$, $C^{4,4}$, and $C^{5,5}$. (e), (f) Intershell rotation melting temperature as a function of ν for different systems at certain interlayer separations ($l=1,1.5$).

C. Intershell rotation melting temperature

For a system consisting of only two shells located one in each of two layers, one of the simplest melting styles is intershell rotation melting. By using the harmonic approximation, we define the melting temperature for the intershell rotation as

$$T_{\mathrm{rm}}^{\sigma\tau} = \delta N_\sigma \left(\sum_i^{N_\sigma} \varphi_i^{-2} \sum_{k=2}^{2N} \frac{1}{S} \sum_{s=1}^{S} \frac{[\phi_i^\sigma(k) - \phi_s^\tau(k)]^2}{\omega_k^2} \right)^{-1}, \quad (6)$$

where $\delta \simeq 0.1$ is the modified Lindemann melting criterion for 2D Wigner crystals [20,35–37], and φ_i is the mean angular interparticle distance for the ith particle in the shell consisting of N_σ particles in layer σ. The sum over s involves the S neighbor particles in shell τ for the ith particle in shell σ. The angular displacement is denoted by

$$\phi_i^{\sigma(\tau)}(k) \simeq \tan^{-1}\left(\frac{\rho_i^{\sigma(\tau)}(k) \cdot \mathbf{c}_i}{|\mathbf{r}_i^{\sigma(\tau)}|} \right), \quad (7)$$

where $\rho_i^{\sigma(\tau)}(k)$ is the displacement vector for the ith particle with mode k in the layer $\sigma(\tau)$ ($\sigma,\tau = A,B$), and $\mathbf{c}_i$ is a unit vector satisfying the relation $\mathbf{r}_i \cdot \mathbf{c}_i = 0$.

Figures 7(a)–7(d) show the intershell rotation melting temperature T_{rm} as a function of the interlayer distance l and the CR for the systems $C^{2,2}$, $C^{3,3}$, $C^{4,4}$, and $C^{5,5}$, respectively. For each system, the range of l is chosen to keep the ringlike configuration (i.e., there is no structural phase transition occurring in the system). From Fig. 7 (for system $C^{2,2}$), we find that T_{rm} decreases with increasing l at a fixed ν due to the reducing intershell interaction. The same characteristics can be also found in Figs. 7(b)–7(d). Figure 7(e) describes T_{rm} as a function of ν at $l=1$. We know that, at small and large values of ν, $T_{rm}^{2,2} > T_{rm}^{3,3} > T_{rm}^{4,4} > T_{rm}^{5,5}$ (in the form of $T_{rm}^{N_A,N_B}$), while that relation is always ensured when l is large enough [e.g., $l=1.5$ as shown in Fig. 7(f)]. This feature means that the two shells with more particles usually have a lower intershell rotation temperature at certain interlayer distances. We also find that, in principle, the ν occurring at the maximum value of T_{rm} is not always $\nu=1$, where intuitionally more energy is needed to excite intershell rotation motion, and there will be a shift toward larger values of ν with increasing l [see also Figs. 7(e) and 7(f)]. This behavior results from the variation of LNFM along with l.

Then we give the T_{rm} for varying l and μ in Fig. 8. Figures 8(a)–8(d) show T_{rm} for the systems $C^{2,2}$, $C^{3,3}$, $C^{4,4}$, and $C^{5,5}$, respectively. We find that at a fixed μ the T_{rm} decreases with increasing l, which is similar to the case of varying the CR. Figures 8(e) and 8(f) show T_{rm} as a function of μ for different l. At a certain interlayer distance [e.g., $l=1$, as shown in Fig. 8(e)], the relation $T_{rm}^{2,2} > T_{rm}^{3,3} > T_{rm}^{4,4} > T_{rm}^{5,5}$ is found in the regions of small and large μ. When l is large enough [e.g., $l=1.5$, as presented in Fig. 8(f)], the relation is always ensured, coinciding with the condition of varying CR. At small interlayer separation, the maximum of T_{rm} corresponds to $\mu=1$, while the peak position will shift toward zero with increasing value of l, which is in contrast to the results for varying ν.

The characteristics of T_{rm} show that intershell rotation melting can be adjusted by varying the CR and MR of the two kinds of particles located in the two layers, as well as the interlayer separation.

IV. CONCLUSION

The normal modes and the melting properties of a bilayer Coulomb system consisting of two kinds of charged particles with different charges or masses located, respectively, in two layers trapped by a parabolic confinement potential are investigated. The particles are kept in ringlike configurations by the use of particular interlayer separations.

For studying the dynamical properties of a 2D Coulomb cluster within a single layer, many setups have been perfectly designed [9,11–15,17,18,23]. The experimental setup we model in this paper can be conceptually realized by two kinds of charged particles trapped each into one of two transparent slippery plates with shallow homocentric circular parabolic troughs. The sketch of the setup is shown in Fig. 9. Even though the ideal setup cannot be immediately applied to experiments for the moment, it will stimulate further experimental research into the characteristics of two-layer systems.

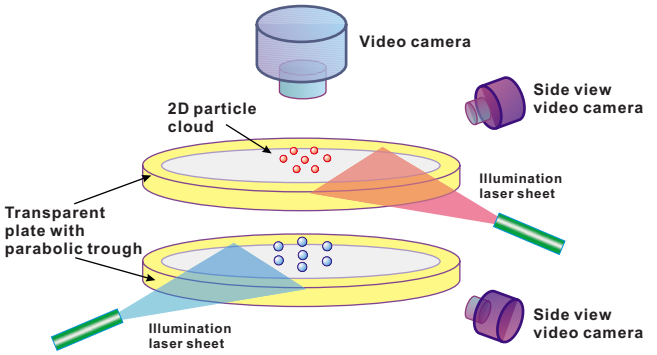

FIG. 9. (Color online) Sketch of the ideal experimental setup. The two kinds of particles are illuminated by laser sheets with different frequencies and described by balls with different colors (gray) and size. They are confined in two parallel transparent slippery plates with shallow homocentric circular parabolic troughs. The particle trajectory is recorded by a video camera from the top. The side view cameras are used to confirm that the particles in each plate are indeed within only a single layer.

The normal modes of the bilayer system are dependent not only on the CR and the MR between the two types of particles but also strongly on the interlayer separation. In principle, when the interlayer separation is small, only at small values and large values of the CR does the first excited state correspond to ISR, while when the interlayer distance is above a critical value, the LNFM corresponds only to ISR no matter the value of the CR. Meanwhile, the corresponding relation is related to the ratio of the numbers of the two kinds of particles in different shells. Similar behaviors also occur in systems consisting of particles with different MRs. Analogous characteristics are also contained in the corresponding relation between the highest excited state and the breathing mode. The shearlike and compressionlike modes of particles with fixed charge and/or mass in one layer can be tuned by varying the charge and/or mass of the particles in the other layer. Because the normal modes can be adjusted by changing the properties of the particles in the other layer at a certain interlayer separation, we expect that the stability and the melting of particles with fixed charge and mass can be adjusted accordingly. Furthermore, the behavior of the intershell rotation melting indicates that a system with more particles has a lower melting temperature; additionally, the temperature can be adjusted by varying the CR and MR of the two types of particles as well as the interlayer separation.

ACKNOWLEDGMENTS

The authors thank A. Melzer and S. Nunomura for valuable discussions. This work is supported by the National Natural Science Foundation of China.

[1] O. Arp, D. Block, A. Piel, and A. Melzer, Phys. Rev. Lett. **93**, 165004 (2004).
[2] J. H. Chu and Lin I, Phys. Rev. Lett. **72**, 4009 (1994).
[3] R. S. Crandall and R. Williams, Phys. Lett. **34A**, 404 (1971).
[4] C. C. Grimes and G. Adams, Phys. Rev. Lett. **42**, 795 (1979).
[5] U. Albrecht and P. Leiderer, Can. J. Phys. **65**, 1536 (1987).
[6] P. Leiderer, W. Ebner, and V. B. Shikin, Surf. Sci. **113**, 405 (1987).
[7] M. Golosovsky, Y. Saado, and D. Davidov, Phys. Rev. E **65**, 061405 (2002).
[8] M. A. Reed and W. P. Kirk, *Nanostructure Physics and Fabrication* (Academic, Boston, 1989).
[9] C. A. Knapek, D. Samsonov, S. Zhdanov, U. Konopka, and G. E. Morfill, Phys. Rev. Lett. **98**, 015004 (2007).
[10] B. Partoens, V. A. Schweigert, and F. M. Peeters, Phys. Rev. Lett. **79**, 3990 (1997).
[11] S. Nunomura, D. Samsonov, S. Zhdanov, and G. Morfill, Phys. Rev. Lett. **96**, 015003 (2006).
[12] S. Nunomura, S. Zhdanov, D. Samsonov, and G. Morfill, Phys. Rev. Lett. **94**, 045001 (2005).
[13] S. Nunomura, J. Goree, S. Hu, X. Wang, A. Bhattacharjee, and K. Avinash, Phys. Rev. Lett. **89**, 035001 (2002).
[14] V. Nosenko, J. Goree, Z. W. Ma, and A. Piel, Phys. Rev. Lett. **88**, 135001 (2002).
[15] A. Melzer, Phys. Rev. E **73**, 056404 (2006).
[16] Y. J. Lai and L. I, Phys. Rev. E **60**, 4743 (1999).
[17] R. Ichiki, Y. Ivanov, M. Wolter, Y. Kawai, and A. Melzer, Phys. Rev. E **70**, 066404 (2004).
[18] M. Klindworth, A. Melzer, A. Piel, and V. A. Schweigert, Phys. Rev. B **61**, 8404 (2000).
[19] V. M. Bedanov and F. M. Peeters, Phys. Rev. B **49**, 2667 (1994).
[20] V. A. Schweigert and F. M. Peeters, Phys. Rev. B **51**, 7700 (1995).
[21] Y. Ivanov and A. Melzer, Phys. Plasmas **12**, 072110 (2005).
[22] Z. W. Ma and A. Bhattacharjee, Phys. Plasmas **9**, 3349 (2002).
[23] A. Melzer, Phys. Rev. E **67**, 016411 (2003).
[24] W. P. Ferreira, F. M. Peeters, and G. A. Farias, Phys. Rev. E **68**, 066405 (2003).
[25] B. Partoens and F. M. Peeters, J. Phys.: Condens. Matter **9**, 5383 (1997).
[26] I. V. Schweigert, V. A. Schweigert, and F. M. Peeters, Phys. Rev. Lett. **84**, 4381 (2000).
[27] M. E. Leunissen, C. G. Christova, A. Hynninen, C. P. Royall, A. I. Campbell, A. Imhof, M. Dijkstra, R. van Roij, and A. van Blaaderen, Nature (London) **437**, 235 (2005).
[28] J. A. Drocco, C. J. Olson Reichhardt, C. Reichhardt, and B. Jankó, Phys. Rev. E **68**, 060401(R) (2003).
[29] K. Nelissen, B. Partoens, and F. M. Peeters, Phys. Rev. E **69**, 046605 (2004).
[30] W. P. Ferreira, F. F. Munarin, K. Nelissen, R. N. Costa Filho, F. M. Peeters, and G. A. Farias, Phys. Rev. E **72**, 021406 (2005).
[31] K. Nelissen, B. Partoens, I. Schweigert, and F. M. Peeters, Europhys. Lett. **74**, 1046C1052 (2006).
[32] G. Goldoni and F. M. Peeters, Phys. Rev. B **53**, 4591 (1996).
[33] X. Lu, C. Q. Wu, A. Micheli, and G. Pupillo, Phys. Rev. B **78**, 024108 (2008).
[34] N. Metropolis, A. W. Rosenbluth, M. N. Rosenbluth, A. M. Teller, and E. Teller, J. Chem. Phys. **21**, 1087 (1953).
[35] F. Lindemann, Phys. Z. **11**, 609 (1910).
[36] V. M. Bedanov, G. V. GVadiyak, and Yu. E. Lozovik, Phys. Lett. **109A**, 289 (1985).
[37] Yu. E. Lozovik and V. M. Fartzdinov, Solid State Commun. **54**, 725 (1985).